Morphological studies of zirconium phosphate nanoparticles as support for Co(II) and Ni(II) catalysts for the OER and ORR

Kálery La Luz-Rivera[1], Mario V. Ramos-Garcés[1], Joel Sanchez[2], Thomas F. Jaramillo[2], Héctor D. Abruña[3], Jorge L. Colón[1]

[1]*Department of Chemistry, University of Puerto Rico, P.O. Box 23346, Río Piedras, P.R. 00931-3346*

[2]*Department of Chemical Engineering, Stanford University, Stanford, California, 94305, USA .*

[3]*Department of Chemistry and Chemical Biology, Cornell University, Ithaca, NY 14853.*

Abastract

The current energetic crisis is promoting the interest in new schemes for renewable energy. Hydrogen has the potential to substitute current methods of energy production which are based on fossil fuels. One way to produce hydrogen in a sustainable fashion is by water electrolysis using the sun as the energy source. Devices that run this process suffer from considerable overpotential losses in the oxidative half of electrolysis, better known as the Oxygen Evolution Reaction (OER). To improve the efficiency of these devices, the energetic loses must be addressed by designing improved electrocatalysts. One general strategy is to support active materials onto supports that engender improve performance. For this reaction, zirconium phosphate (ZrP) has proven to be a catalyst support for transition metals. ZrP nanoparticles used for studies on this reaction are hexagonal shaped. In this study we modified the ZrP morphology. ZrP rods, cubes and spheres were synthetized and used as support for Co(II) and Ni(II) cations. Their structure and activities were analyzed and compared with those of the hexagonal morphology. Characterization of the materials were performed with transmission electron microscopy (TEM), X-ray powder diffraction (XRPD) and Fourier transform infrared spectroscopy (FT-IR) to confirm that the desired morphologies were achieved. The activity was assessed with cyclic voltammetry and the obtained overpotentials were 0.491 V, 0.522 V, 0.490 V, 0.547 V for the samples Co(II):ZrP hexagonal, Co(II):ZrP rods, Co(II):ZrP cubes, and Co(II):ZrP spheres, respectively. The Ni(II): ZrP hezagonal, Ni(II): ZrP rods, Ni(II): ZrP cubes, and Ni(II): ZrP spheres samples had overpotencials of 0.592 V, 0.504 V, 0.430 V, 0.462 V respectively. Double-layer capacitance measurements were performed to further characterize the activity of the materials. Chronopotentiometry was also performed to measure the stability of the materials; Co(II):ZrP cubes and Ni(II): ZrP Cubes showed stability for two hours. Based on these findings, ZrP cubes show promising potential as support for catalysts for the OER. Oxygen reduction reaction (ORR) studies were also performed to see if these materials could work as bifunctional catalysts. However, it showed to be active at the half way potential of the commercial Pt catalyst, which means they work for the two-electron process of the ORR and produces hydrogen peroxide as a product. They do not perform the four-electron process at which Pt works without producing hydrogen peroxide as a product.

Introduction

Today our energy resources are based on the use of fossil fuels. Scientists estimate that we have over 2,000 years of use of these resources.[1] However combustion of these fuels produce carbon dioxide. Carbon dioxide is a greenhouse gas that causes thermal energy to stay on the atmosphere which increases the temperature on earth causing what it is known today as global warming. Furthermore, there has been research to develop new ways of energy production that decrease carbon dioxide emissions into the atmosphere. Some of this new energy sources are geothermal, hydraulic, biomass, wind, and solar power. Nevertheless, some of this energy sources still produce carbon dioxide, do not work efficiently enough to satisfy our energy demand or are very expensive. For them to be used on a bigger scale and make one of these our main energy source, these factors must be addressed.

An option that was developed for the production of energy was solar water-splitting cells. In these solar water-splitting cells, like the name suggest, water is split into hydrogen and oxygen by a light source which is the sun. This reaction occurs though two half reactions, the oxygen evolution reaction (OER; Fig 1.a) and the hydrogen evolution reaction (HER; Fig 1.b).

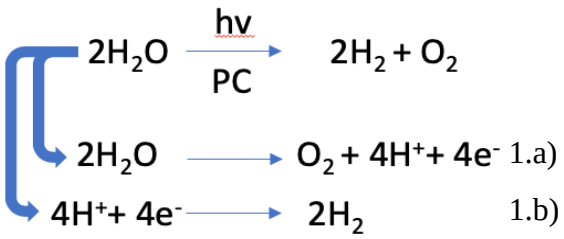

Figure 1. The water-splitting reaction and its half-cell reactions.

The renewable, sustainable production of hydrogen could have many benefits, displacing the conventional fossil-based processes for its production and use in the fuels and chemical industry, and potentially serving as an alternative energy vector given its high gravimetric energy density and modularity of use.[2] Hydrogen today is used in fuel cells to produce electrical current, however the hydrogen used on these cells comes mostly from steam methane reforming which produces CO_2 emissions. Nevertheless, the hydrogen produced in water-splitting cells, by the reaction showed (Fig. 1), can later be used on fuel cells to produce an electrical current without having CO_2 emissions into our environment., the oxygen evolution reaction makes this process kinetically hindered. This reaction has a slow rate, a major loss of energy because of its four electrons oxidation. Its high oxidative environment causes the electrode where it occurs to corrode and decrease in performance over time. Researchers are looking for ways to improve the issues that OER presents. One way of improving this reaction on a water-splitting cell is improving the electrocatalysts. Finding a better electrocatalyst for will improve the kinetic barriers of the reaction. Today, decent electrocalysts for OER like RuO_2 and IrO_2 are commercially available, nevertheless these are made of expensive and non-abundant metals, and they do not perform at the expected overpotentials for the reaction. It is desired to improve even further the electrocatalysts by using transition metals that are earth-abundant, inexpensive and active for the OER. To develop these electrocatalysts, catalyst design techniques have been developed.

These techniques include encapsulation and changes in morphology using support materials. Zirconium phosphate (ZrP) has been identified as a potential support to do this.

Figure 2

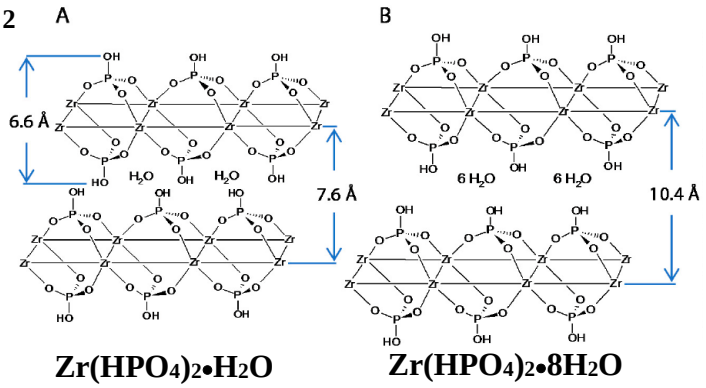

Zirconium phosphate is an inorganic laminal material where the zirconium atoms are aligned on an imaginary plane and these are connected by phosphate groups alternated on the upper and lower part of the plane. Three oxygen atoms of the phosphate group bond to three different Zr^{4+} ions; six oxygen atoms from different phosphate groups coordinate the Zr atoms forming an octahedral coordination symmetry around each zirconium ions.[3] The fourth oxygen of the phosphate groups is connected to a hydrogen atom that can later on be substitute with cationic species. Two common phases of ZrP are Θ-ZrP (Fig 2.B) and α-ZrP (Fig 2.A). From past research conducted by our laboratory it has been concluded that in the Θ-ZrP phase the transition metals are absorbed on the surface and intercalated in the interlaminar space of zirconium phosphate. However, in α-ZrP transition metals are only absorbed on the surface, not intercalated. Both of these phases were studied modifying them with the transition metals Co(II), Fe(II) Fe(III) and Ni(II) to see their activity for OER. The catalysts modified with cobalt and nickel present more stability under OER conditions. The α-ZrP phase modified with Co(II) and Ni(II) worked efficiently for the OER, this phase decreased the overpotential more significantly than the Θ-ZrP. This difference between these two phases is due to that α-ZrP contains more active material absorbed on the surface for OER than the Θ-ZrP in which the material is mostly intercalated than on the surface.

For this project we decided to modify the morphologies of ZrP and study the effects of the changes on its catalytic activity for OER. The morphologies synthetized where α-ZrP (hexagonal shape), ZrP cubes, ZrP rods and ZrP spheres. We modified each one of this with the metal ions of Co(II) and Ni(II). Electrochemical and chemical-physical characterization studies where done to see their structure and activity.

Also, oxygen reduction reaction (ORR) studies where done to see if these catalysts are active for it. If they are active for the oxygen reduction reaction, these catalysts could be used in fuel cells to produce electrical current with the use of oxygen and hydrogen, with water and heat being the only byproducts. These catalysts, if efficient, they can be a substitute for the commercial platinum catalyst that nowadays is used for the ORR.

Methodology

Synthesis of ZrP morphologies

To synthesize the α-ZrP, $ZrOCl_2 \cdot 8H_2O$ was mixed with 6 M H_3PO_4 at 94°C for 2 days under constant stirring. It was washed and rinsed and the result was θ-ZrP, this was left drying under vacuum at room temperature. After drying, α-ZrP was the final product. To synthesize the ZrP cubes morphology, zirconyl propionate was dissolved in ethanol. Phosphoric acid was added to the solution at room temperature while stirring. The solution starts becoming a gel. The gel was washed with ethanol and dried in an oven at 120 °C. To synthesize ZrP rods, $ZrOCl_2 \cdot 8H_2O$ was mixed with NH_4F in a 1:1 F:Zr molar ratio. H_3PO_4 (85%) was added to the solution in a 3:1 H_3PO_4:Zr molar ratio while mixing. To synthesize the zirconium phosphate spheres $ZrOCl_2 \cdot 8H_2O$ was dissolved in water. $(NH_4)_2CO_3$ was added and waited until the solution turned clear. $(NH_4)_2PO_4$ and TTBr where added. The solution was stirred and placed in oven at 80 °C for 3 days. The precipitate was transferred into an autoclave and heated at 90 °C for 2 days. The temperature was increased to 120 °C for 1 day. Lastly, it was washed with H_2O and calcined in a furnace at 540 °C for 6 h.

Ink Preparation and Electrochemical Measurements

Each catalyst ink was prepared by dispersing 5 mg of the catalyst and 2.5 mg of carbon black in 2.55 mL of isopropanol and 10.02 μL of Nafion 117. The ink was sonicated until it was well dispersed (ca. 30 mins). Electrochemical measurements were performed on a VMP3 potentiostat/galvanostat (BioLogic Science Instruments). Oxygen evolution catalytic studies were carried out on a three-electrode electrochemical cell using a rotating disk electrode (RDE) assembly (Pine Research Instrumentation). OER measurements were performed between 0.2 and 1.0 V versus the silver/silver chloride couple (Ag/AgCl) at 20 mVs^{-1} in O_2-saturated 0.1 M KOH electrolyte with an Ag/AgCl reference electrode (Fisherbrand accumet Glass Body Ag/AgCl Reference Electrode – Mercury-Free, Thermo Fischer). The counter electrode was a platinum wire and the working electrode was a clean, mirror finish-polished, 5 mm diameter glassy carbon disk (GCD) modified with the metal-modified ZrP catalysts. Modification of the GCD with the ZrP catalysts was performed by spin drying a 10 μL drop of an isopropanol, carbon black, Nafion 117, and ZrP catalyst ink at 600 rpm. After drying, the working electrode was composed of a thin coating of the material supported onto the GCD. The total catalyst loading of the working electrode was 100 $\mu g/cm^2$ of material, including the ZrP support. During electrochemical measurements, the working electrode was rotated at 1600 rpm. The rotation speed was fast enough to help in product removal from the surface and limit the bubble formation from oxygen evolution. The solution resistance of the cell was measured at 100 kHz with 20 mV amplitude about the open-circuit potential (OCP), and *i*R-drop compensation occurred after electrochemical testing. The typical solution resistance varied from 40 to 50 Ω. All potentials were converted and reported herein versus the reversible hydrogen electrode (RHE).

The mass normalized activities were determined at 1.73 V (0.5 V of overpotential) and assumed that all metal atoms are electrochemically active and participating in the OER. The catalytic activity was also determined through a Tafel

analysis. Tafel plots were constructed for each system from voltammetry data. The Tafel slopes were determined from the linear region of the plot.
The stability of the catalysts was studied with chronopotentiometry (CP). The working electrode was polarized to a current of 10 mA/cm^2 for Co-modified samples and at 2 mA/cm^2 for Ni-modified samples. The potential necessary to hold these currents were measured as a function of time.

The double-layer capacitance (C_{DL}) for each system was determined from cyclic voltammetry (CV). The non-Faradaic region was identified from an initial CV. For our systems, the region used was from 0.1 V to 0.4 V vs Ag/AgCl and the potential was swept from the more negative potential to the more positive potential and back at 7 different scan rates: 0.02, 0.05, 0.10, 0.15, 0.20, 0.25, and 0.30 Vs^{-1}. The working electrode was held at each potential vertex for 10 s before beginning the next sweep. C_{DL} was measured by plotting the non-Faradaic current (j_a-j_c/2) versus the scan rate and extracting the slope of the linear best-fit line. The value of j_a and j_c were chosen at 0.3 V vs Ag/AgCl and all current at this potential is assumed to be due to double-layer charging.

Electrochemical measurements for ORR were made using a three-electrode electrochemical cell in a rotating disk electrode (RDE) setup (Pine Research Instrumentation). The working electrode was an ink-modified GCD mounted in the RDE, the counter electrode was a platinum rod and the reference electrode was an Ag/AgCl electrode, the electrolyte was 0.1 M KOH. The disk used on the RDE was a mirror-polished, 5 mm diameter glassy carbon disk (GCD) with the catalyst spin dried on top. To conduct the experiments, a VMP3 potentiostat/galvanostat (BioLogic Science Instrument) was used. First, the electrolyte was bubbled with argon to develop an inert atmosphere inside the cell. CV was conducted to see if the materials reacting were the catalyst. The potential was swept from 0.2 mV to -0.4 mV vs Ag/AgCl at 15 mV/s. Later, the electrolyte was saturated bubbling with oxygen for 15 min. Then, linear sweep voltammetry (LSV) was conducted from 0 mV and -0.6 mV vs Ag/AgCl at a sweep rate of 5 mV/s while the electrolyte was saturated with O_2 and the working electrode rotated at 1600 rpm.

Physical and Chemical Characterization

X-ray powder diffraction (XRPD) data was obtained using a using Rigoku Ultima IV X-ray diffractometer. The *d* spacing was calculated using Bragg's law ($n\lambda=2d_{hkl}\sin\theta$), where λ is the wavelength of the X-ray source, d_{hkl} is the interlayer distance between planes in the unit cell, and θ is the diffraction angle. The morphology of the ZrP nanoparticles was studied by transmission electron microscopy/scanning transmission electron microscopy using a FEI Tecnai (Thermo Fisher Scientific, Inc.) G2F20 TEM/STEM microscope operated at 200 kV. Quantitative determination of the cobalt and nickel loading on the modified ZrP catalysts was done by inductively coupled plasma mass spectrometry (ICP-MS) measurements. All samples were digested in an aqua regia matrix overnight and were diluted and filtered to a 5 vol % acid concentration for analysis. Vibrational spectroscopy data was obtained from 4000 to 400 cm^{-1} using a Bruker (Bruker Optics, Massachusetts, USA) Tensor 27 FT-IR spectrometer with Helios ATR attachment containing a diamond crystal.

Results and Discussion

Figure 1 shows FT-IR spectra of α-ZrP, ZrP rods, ZrP spheres, ZrP cubes. We can see the four peaks associated with lattice water on the spectrum of α-ZrP. Three of these peaks are sharp and small at ca. 3600, 3500 cm^{-1}, and 1600 cm^{-1}; the fourth peak is broad at ca. 3150 cm^{-1}. However, the peaks in the FT-IR spectra of ZrP cubes and ZrP spheres do not show these peaks and this is due to the high temperatures in which they are synthetized at which make the water to evaporate from the sample. The peaks at the region of 1057-966 cm^{-1} are from the symmetric and antisymmetric orthophosphate group vibrations, with these peaks we know that we have successfully synthetized ZrP.

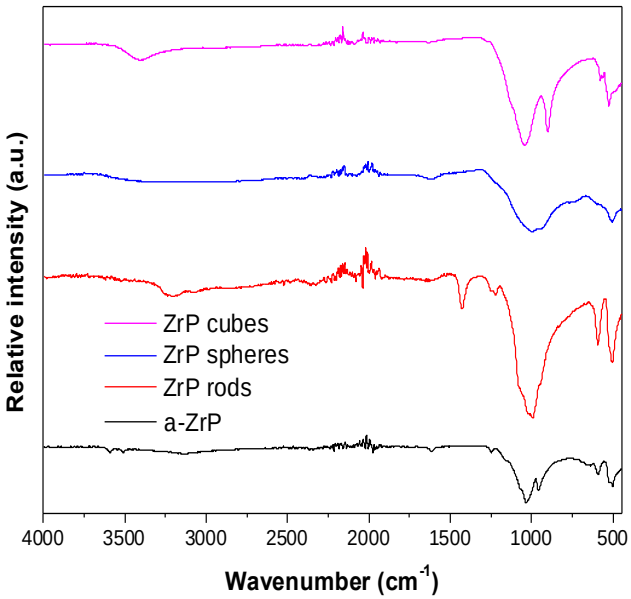

Figure 1. FTIR spectra of α-ZrP, ZrP rods, ZrP spheres, ZrP cubes.

To further characterize the samples, XRPD was. The usual peaks characteristic of α-ZrP at 11.6° and ca. 34° can be seen (Figure 2). The peak at 11.6° represents the interlaminar distance between the layers of ZrP (7.6 Å). Also, the diffraction pattern of ZrP rods is similar to that of α-ZrP suggesting that the alignment of ZrP layers is the same between these two. Nevertheless, the XRPD patterns related to ZrP cubes and ZrP spheres do not look similar to the pattern of α-ZrP (Figure 2). The diffraction pattern of the ZrP cubes correlates well with that of previously published data, indicating that the cube-like phase of ZrP was successfully synthetized. The ZrP spheres is a mesoporous material which do not present diffraction peaks except at very low angles < 2º. The diffractometer used can make measurements from 3º, meaning that now features are expected to be observed.

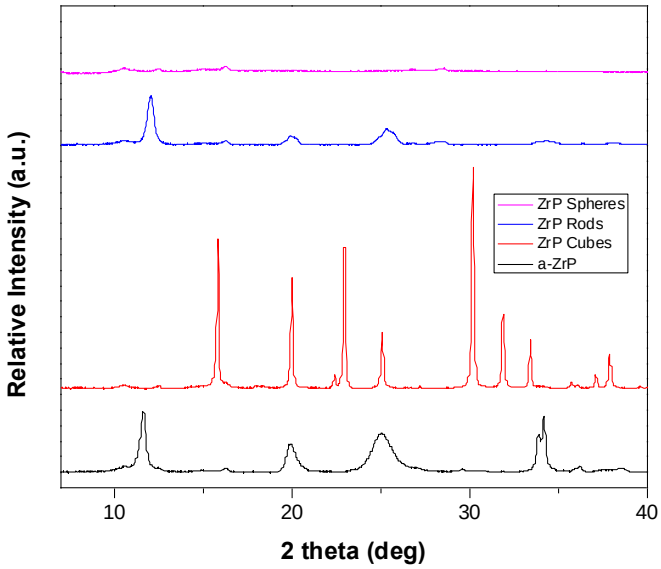

Figure 2. XRPD of α-ZrP, ZrP cubes, ZrP rods, and ZrP spheres.

XRPD was also performed for the ZrP morphologies modified with the metal ions Co(II) and Ni(II). These were used as verify that the morphology of the support does not changed during the modification step. As the catalysts were not processed further (e.g., with heat treatments), the form of the metal resulting on the surface of ZrP is amorphous and, as expected, no diffraction corresponding to those metals is observed by XRPD. The peak at 11.6° for α-ZrP and ZrP rods was used as a reference to see if a change in interlaminar space between the samples. If some displacement is generated in this peak (to the left) it means that intercalation occurred. The Co/ZrP rods and Ni/ZrP rods patterns (Figure 3c) showed the same peak patterns than ZrP rods and α-ZrP, meaning also that the materials were absorbed and not intercalated. Lastly, the XRPD patterns Co/α-ZrP and Ni/α-ZrP (Figure 3a), showed the characteristic peaks of α-ZrP without any changes in its peak that represent the interlaminar space at 11.6°.

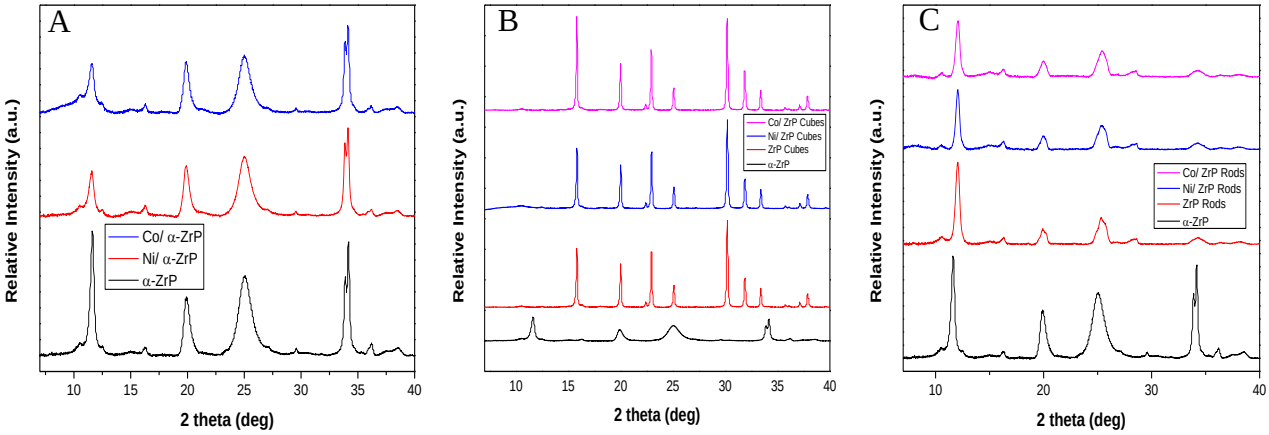

Figure 3. XRPD diffraction patterns of **A)** α-ZrP samples **B**) ZrP cubes samples **C**) ZrP rods samples.

Transmission electron microscopy was also performed to see if the morphologies desired were synthetized**.** α-ZrP (Figure 4) had an hexagonal morphology and measurements of 100 nm and 200 nm. The ZrP cubes (Figure 5) had measurements between 100 nm and 200 nm. The ZrP rods (Figure 6) had lengths ranging from 400 nm to 800 nm and a diameter approximately of 100 nm. The measurements of the ZrP spheres (Figure 7) were between 1.5 and 3 microns.

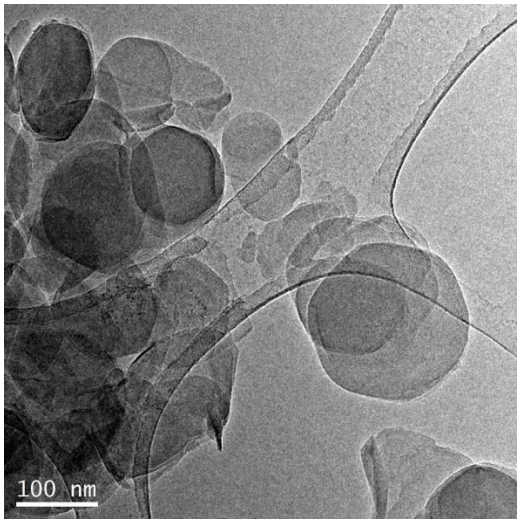

Figure 4. α-ZrP

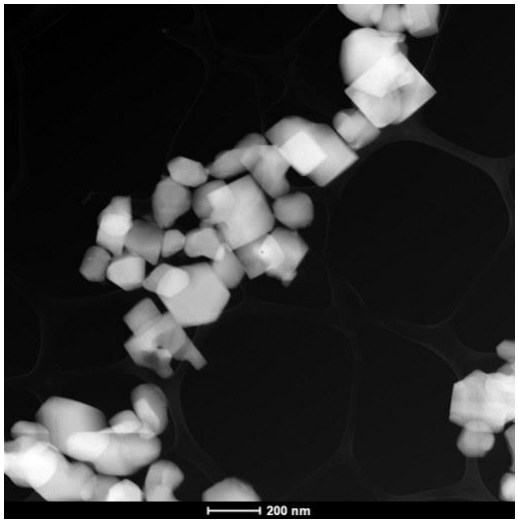

Figure 5. ZrP cubes

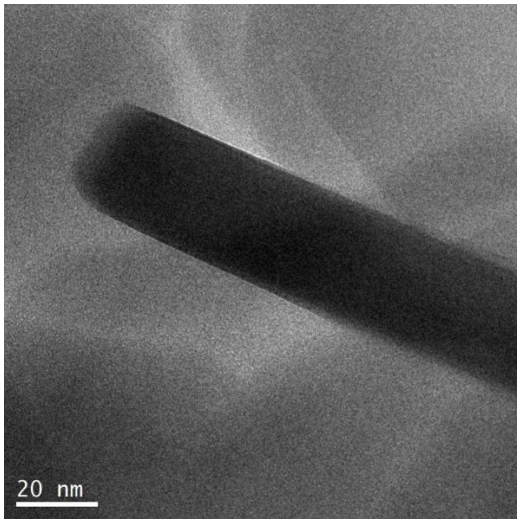

Figure 6. ZrP rods

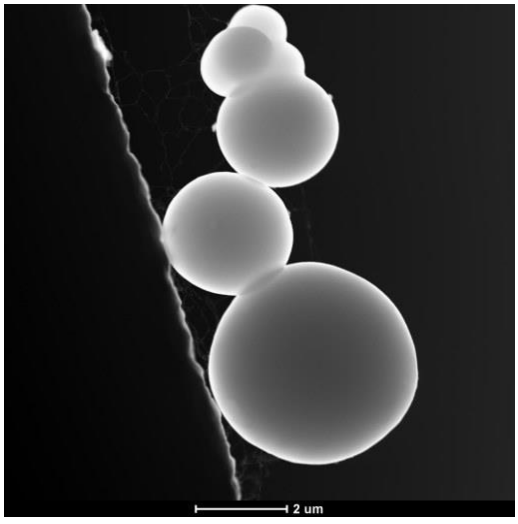

Figure 7. ZrP cubes

Electrochemical measurements (Figures 8a and 8b.) were also perform on the samples to measure how active they are for the OER. The ZrP modified cubes showed lower overpotentials 0.490 V for Co/ZrP cubes and Ni/ZrP cubes with 0.430 V. Co/α-ZrP and Ni/α-ZrP showed overpotentials of 0.491 V and 0.592 V respectively. The Co/ZrP rods had overpotentials of 0.522 V and Ni/ZrP rods of 0.504 V.

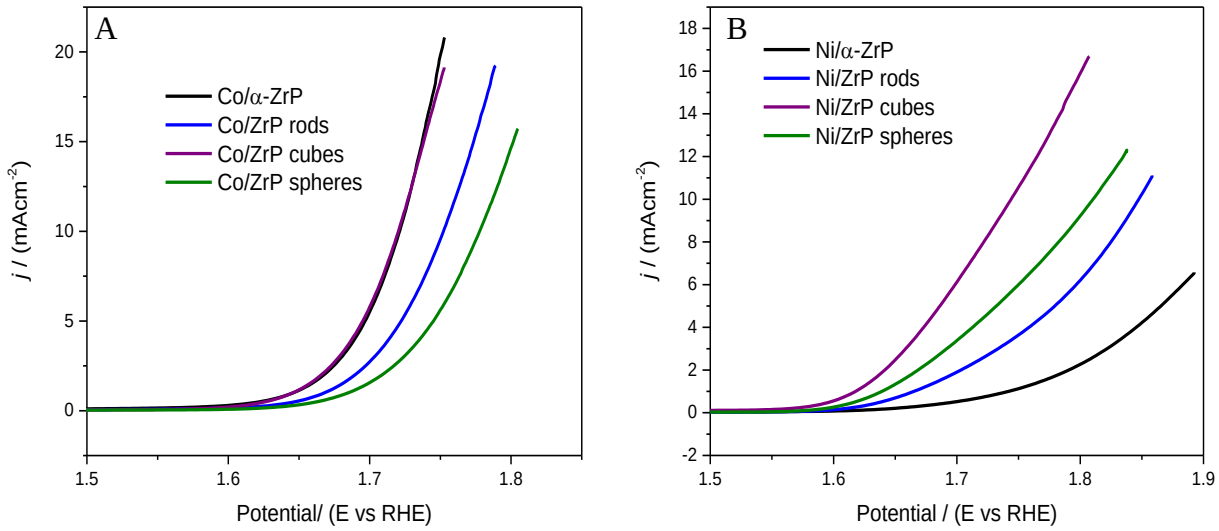

Figure 8. Electrochemical data for oxygen evolution reaction A) ZrP morphologies modified with Co(II). B) ZrP morphologies modified with Ni(II).

Chronopotentiometry was also performed (Figure 9a, 9b) the study the stability of our catalysts. The ZrP cubes morphologies modified with Co(II) and Ni(II) showed to be stable for two hours of electrolysis each and they did not fluctuate the potential at what they work at a current of 10 mA/cm^2 for Co/ZrP cubes and at 2 mA/cm^2 for Ni/ZrP cubes.

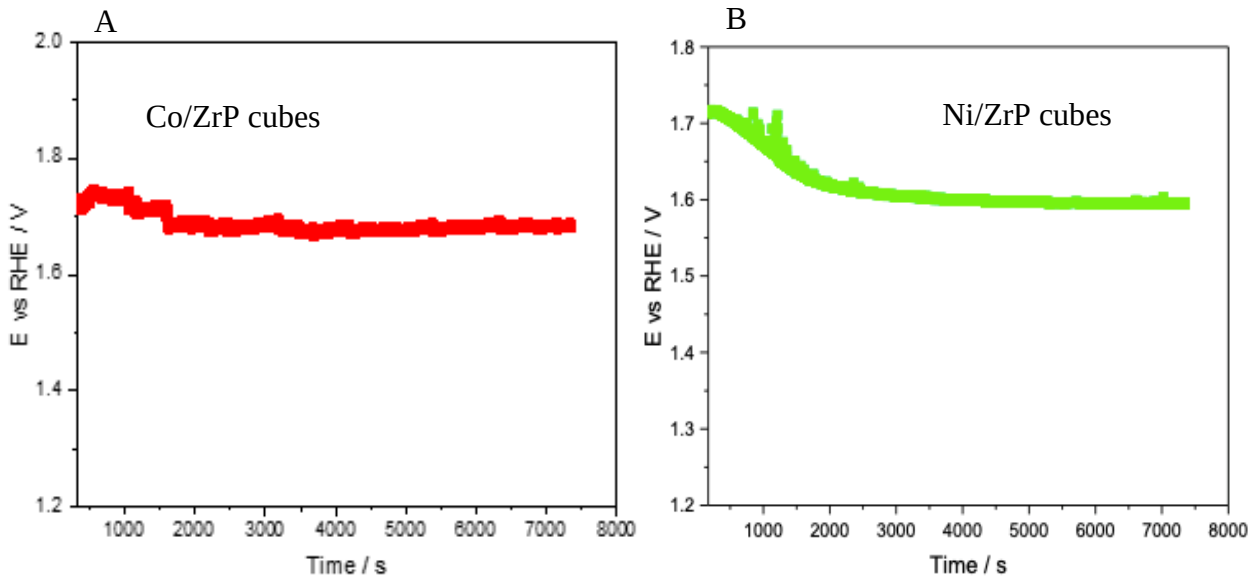

Figure 9. Chronopotentiometry A) ZrP cubes modified with Co(II). B) ZrP cubes modified with Ni(II).

We also performed ORR electrochemical measurements (Figure 10a, 10b). For these, the half-wave potential obtained did not meet with the one expected for the four electron reaction of ORR. The half-wave potentials for Co/α-ZrP, Co/ZrP cubes and Co/ ZrP rods, were 0.612 V, 0.642 V, 0.622 V, respectively. For the morphologies modified with Ni were 0.707 V, 0.710 V, 0.720 V for Ni/α-ZrP, Ni/ZrP cubes and Ni/ ZrP rods, respectively. Their diffusion current fluctuates between -2.30 mA/cm^2 and -2.50 mA/cm^2 for the Co/ZrP morphologies and from -1.85 mA/cm^2 and -2.70 mA/cm^2 for the Ni/ZrP morphologies. The catalysts are active for the two electron reaction of ORR in alkaline media, it produces mostly hydrogen peroxide than water as a product.

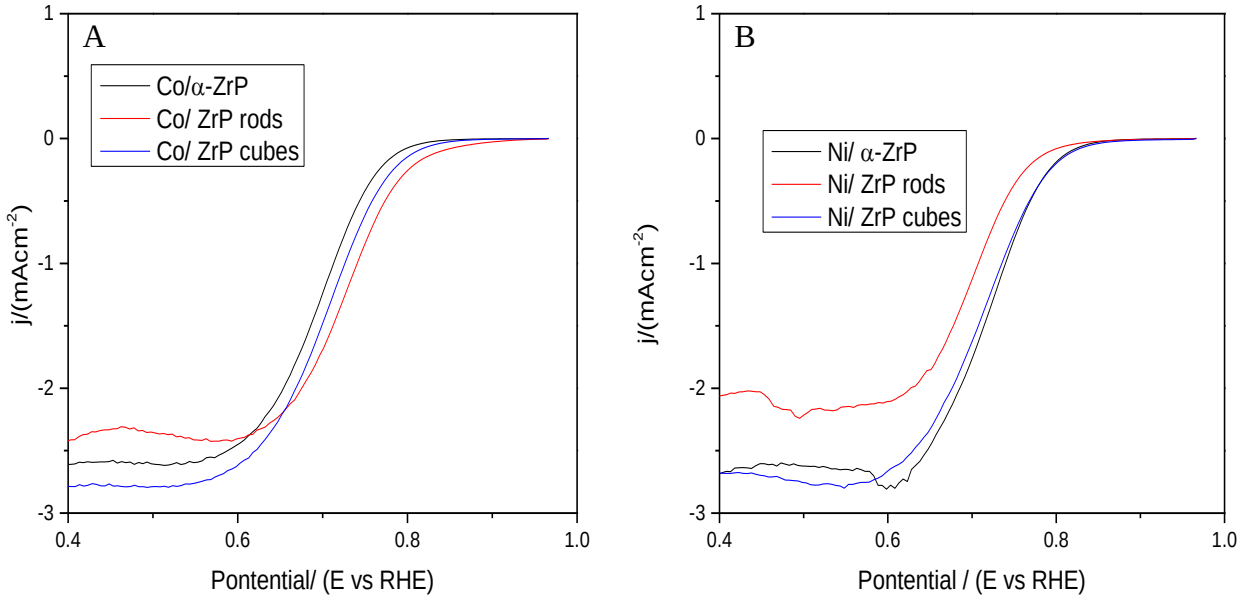

Figure10. LSV for oxygen reduction reaction A) ZrP morphologies modified with Co(II). B) ZrP morphologies modified with Ni(II).

Conclusion

For the oxygen evolution reaction, the different metal modified zirconium phosphate morphologies showed to be active. The cubes morphologies were the ones that showed lower overpotentials, better stability and durability. For further studies, the structure of the cubes will be analyzed to see why these are more stable than the other morphologies. Between the metals absorbed on the surface of the different ZrP morphologies, Ni and Co, cobalt showed better activity. For the studies of oxygen reduction reaction, the catalysts did not showed to be active for the four electron process of ORR, but they were active for the two electron process. They are not efficient for ORR since it produces hydrogen peroxide as a product.

Acknowledgments

We want to thank Daniel Del Toro and Dr. Eduardo Larios for their assistance during this project and Dr. Mahdi Ahmadi for his help. This work was sponsored by NSF-PREM CIE2M program (Award#1827622) and by the NSF Center for Chemical Innovation in Solar Fuels CHE-1305124.

References

1. Lewis, N. S.; Nocera, D. G. *Proc. Nat. Acad. Sci.* **2006,** *103*, 15729-15735
2. Ursua, A; Gandia, L. M.; Sanchis, P. Hydrogen production from water electrolysis: Current status and future trends. Proc. IEEE **2012**, 100, 410–426.
3. Sanchez, J.; Ramos-Garcés, M.V.; Narkeviciute, I.; Colón, J.L.; Jaramillo, T.F. Transition metal-modified zirconium phosphate electrocatalysts for the oxygen evolution reaction. Catalysts *7*, **2017**, 32.

Additional Data Supplements

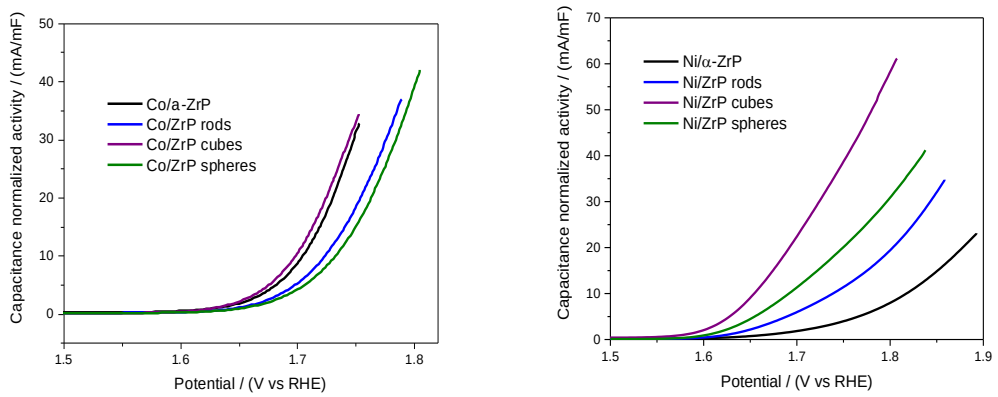

Figure 1. Current normalized by capacitance for the different catalysts.

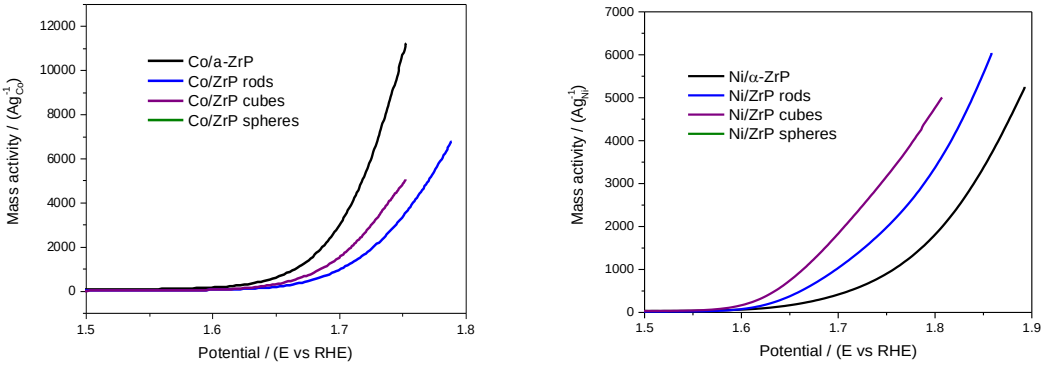

Figure 2. Current normalized by mass for the different catalysts.

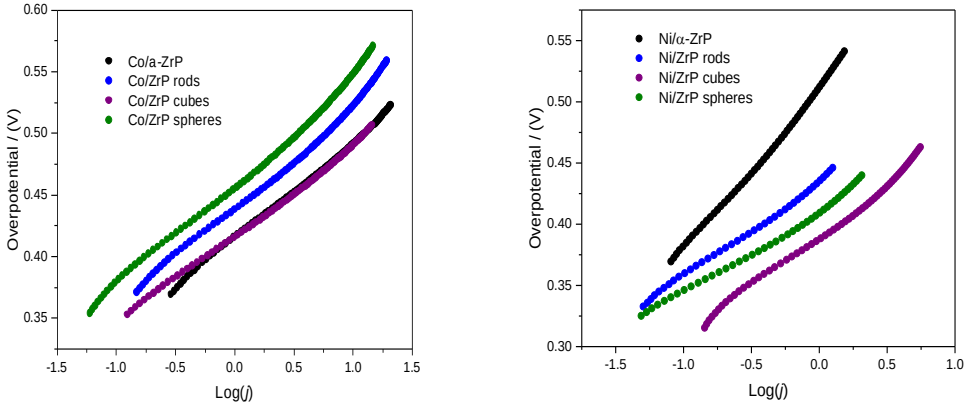

Figure 3. Tafel slope for the different catalysts.